ISSN: 0975-8585

Research Journal of Pharmaceutical, Biological and Chemical Sciences

Using $Ti_{1-x}Al_xN$ Coating to Enhance Corrosion Resistance of Tool Steel in Sodium Chloride Solution.

AL Kameneva[1]*, VI Kichigin[2], TO Soshina[3], and Karmanov VV[1].

[1] Perm National Research Polytechnic University, Department of Innovative Engineering Technology, Komsomol'skii pr. 29, Perm, 614990, Russia.
[2]Perm State University, Research Laboratory of Electrochemistry and Corrosion, Bukireva st. 15, Perm, 614990, Russia.
[3]Perm National Research Polytechnic University, Laboratory of Metallurgy Lenin st. 2, Perm Krai, Lys'va, 618900, Russia.

ABSTRACT

A study has been conducted to find out how the morphological properties, phase composition and ultimate composition of $Ti_{1-x}Al_xN$ coatings applied to samples made of tool steel under various process conditions of pulsed magnetron sputtering influence their corrosion and electromagnetic behaviour in 0.3% NaCl solution. A dense column coating with diameter of crystallites 20-50 nm was formed in optimal power magnetron sputtering system and the ratio of nitrogen and argon gas mixture. The corrosion current density of tool steel decreased with increasing Al content and a volume content of the main ternary phase h-$Ti_3Al_2N_2$ in the $Ti_{1-x}Al_xN$ coating. It is established that Ti0,62Al0,38N coatings containing 86 % $Ti_3Al_2N_2$ phase and 26,5 at.% Al leading to decrease in corrosion current density of tool steel by 43 times and to increase in polarization resistance by 51 times. $Ti_{0,62}Al_{0,38}N$ coating is useful for hardening of bio-medical materials.

Keywords: $Ti_{1-x}Al_xN$ coating, corrosion resistance, bio-medical material, impedance

Corresponding author

ISSN: 0975-8585

INTRODUCTION

Using corrosion-resistant coatings to protect cutting tools and friction pairs (CT&FP) allows us to expand the application scope of their materials due to the protective properties of such coatings against wear, oxidisation and corrosion. One of the modern trends in CT&FP corrosion control is to apply coating by physical vapour deposition (PVD process), which results in low corrosion rates. TiN coatings continue to play an important role. However, $Ti_{1-x}Al_xN$ and $Cr_{1-x}Al_xN$ multi-layer three-component coatings have a greater hardness and greater oxidation resistance [1-4]. High corrosion resistance of aluminum-bearing coatings is due to the presence of aluminum in the top coat. Aluminum aggregates with oxygen and forms a strong protective layer of Al_2O_3, preventing further oxidation of the coating, reducing the corrosion rate and stabilizing the CT&FP material.

Recent publications emphasise the influence of growth defects in PVD-coatings on corrosion resistance of substrate-coating systems [1, 5], therefore more research is required to establish connection between coating deposition and structure formation on the one hand and their protective properties on the other hand. This paper examines the corrosion behaviour of tool steel with $Ti_{1-x}Al_xN$ coatings of various ultimate and phase compositions, applied by pulsed magnetron sputtering (PMS) at various process temperatures in 0.3% solution of NaCl in water. Corrosion resistance of three-component $Ti_{1-x}Al_xN$ coatings was compared with that of two-component TiN coatings.

EXPERIMENTAL

$Ti_{1-x}Al_xN$ coatings on test samples made of X12M tool steel were applied on a UNICOAT-600 PMS unit by current discharge to Al targets at - 14.8 Amp, negative bias voltage on substrate at - 50 V, power of the magnetron sputtering system (MSS) at - 11.5 to 15 kW and gas mixture pressure at- 0.28 Pa. The variable composition of the gas mixture and MSS power are given in Table 1. To determine the influence of PMS process conditions on the structure, phase composition, ultimate composition and, as a result, corrosion resistance of $Ti_{1-x}Al_xN$ coatings, coatings 1, 3 and 6 were applied with constant nitrogen content in the gas mixture (N_2=12%) and variable PMS power, while $Ti_{1-x}Al_xN$ coatings 1-2 and 3-4-5 were applied at permanent PMS power of 15 kW and 14.5 kW respectively and at a variable ratio of gases in the gas mixture.

Table 1: Composition of the gas mixture used in application of $Ti_{1-x}Al_xN$ coatings

Coating no.	MSS power, kW	Nitrogen content, %
1	15.0	12
2	15.0	10
3	14.5	12
4	14.5	7
5	14.5	10
6	11.5	12

The phase composition of $Ti_{1-x}Al_xN$ coatings was determined from diffraction patterns created by Cu Kα radiation using a Shimadzu XRD-6000 X-ray diffractometer. Phase changes in coatings were assessed from volume content of the incoming phases: $Ti_3Al_2N_2$, TiN and AlN_{cub}. To determine the volume contents of incoming phases, the total area of diffraction peaks was taken as 100% and the total area of diffraction peaks of each respective phase was compared with the total area of all phase peaks. The microstructure and chemical composition of appled coatings were studied on a BS 300 scanning electron microscope used in conjunction with EDAX Genesis 2000 tool for microanalysis. The thickness of $Ti_{1-x}Al_xN$ и TiN coatings was determined from cross-sections using the BS 300 microscope.

The $Ti_{1-x}Al_xN$ and TiN-coated samples submitted for electrochemical measurements were potted in epoxy in such a way as to leave exposed only one surface of each coated sample. All measurements were taken at room temperature (between 20°C and 22°C) inside a three-electrode cell filled with unstirred 0.3% NaCl solution affected by natural aeration. NaCl solutions were prepared using high-grade chemicals and deionised water.

ISSN: 0975-8585

An 'open-circuit-potential/time' curve was built for each sample steeped in solution. The impedance spectrum was measured at fixed intervals of time, at E_{cor} corrosion potential, in the f frequency range from 10000 Hz to 0.01 Hz, at 10 mV alternating signal amplitude, on Solartron 1287/1255 (Solartron Analytical). For some coatings, the impedance spectra readings were taken for a range of anodic polarizations. Voltages were measured relative to the saturated silver-chloride electrode and recalculated relative to the standard hydrogen electrode.

RESULTS AND DISCUSSION

Table 2 lists the morphology, phase composition and ultimate composition of formed $Ti_{1-x}Al_xN$ coatings. One can see from Table 2 and Figure 1 that the composition and morphology of $Ti_{1-x}Al_xN$ coatings depend on the process conditions in which their deposition takes place (MSS power and reaction-gas content (N_2) in the gas mixture).

Table 2: Thickness, morphology, phase composition and ultimate composition of coatings (δ - coating thickness)

Coating no.	δ, μm	$Ti_{1-x}Al_xN$ coating structure	Volume contents of incoming phases, %			Ultimate composition of $Ti_{1-x}Al_xN$ coating
			$Ti_3Al_2N_2$	TiN	AlN_{cub}	
1	1.0	Dense ordered columnar defect-free structure, crystallite size 20 to 50 nm	86	10	4	$Ti_{0.62}Al_{0.38}N$
2	2.3	Uneven discontinuous cellular structure with isolated polycrystalline formations	59	27	14	$Ti_{0.75}Al_{0.25}N$
3	1.4	Dense ordered columnar structure, crystallite size 5 to 45 nm	65	26	9	$Ti_{0.65}Al_{0.35}N$
4	2.5	Large-cell defective structure with scattered 3D formations of low cohesive strength	56	43	1	$Ti_{0.77}Al_{0.23}N$
5	1.0	Dense ordered defect-free structure with isolated 3D formations and surface defects, crystallite size 50 to 100 nm	60	31	9	$Ti_{0.67}Al_{0.33}N$
6	2.8	Uneven large-cell structure with multiple surface discontinuities	51	44	5	$Ti_{0.95}Al_{0.05}N$

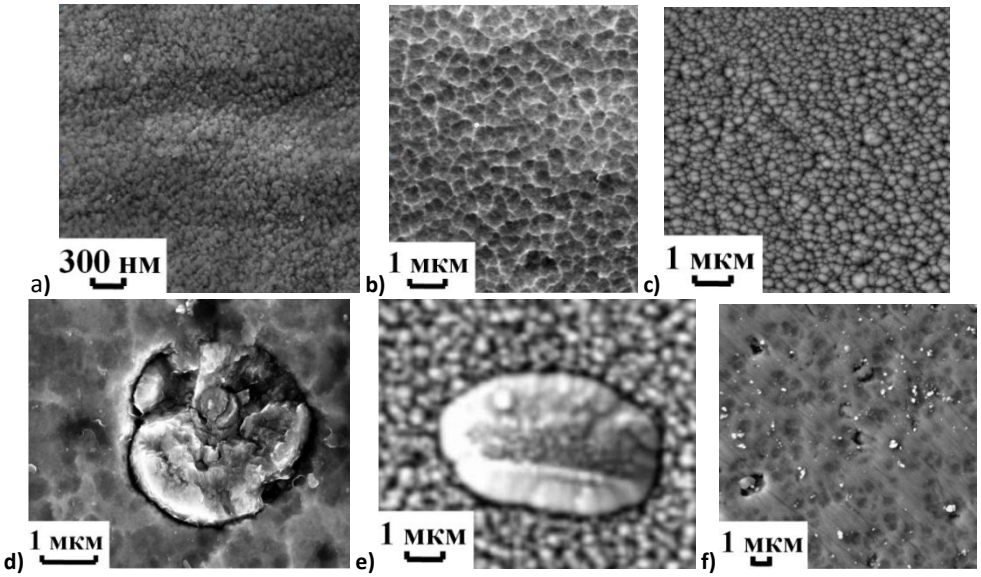

Figure 1: Morphology of $Ti_{1-x}Al_xN$ coated surfaces: a) 1, b) 2, c) 3, d) 4, e) 5, f) 6

The corrosion and electrochemical behaviour of $Ti_{1-x}Al_xN$ and TiN coatings were assessed from the readings of impedance and polarization measurement. Figure 2 shows the curves for impedance of substrate

ISSN: 0975-8585

material – X12M steel. The shape of the Nyquist plots is close to a semicircle with the centre below the X axis. The Bode plots are symmetrical in shape. The impedance of X12M steel in 0.3% NaCl solution declines in time.

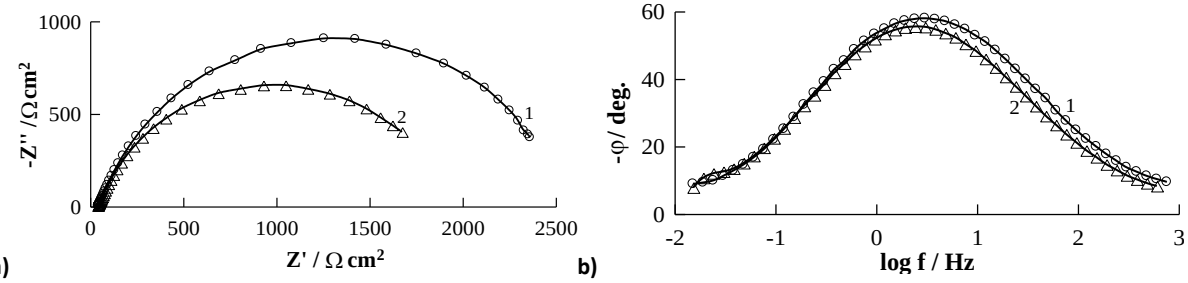

Figure 2: Nyquist plots (a) and Bode plots (b) for X12M steel in 0.3% NaCl solution under corrosion potential. Electrode exposure time, hrs: 1 plot – 1; 2 plot – 2

Figure 3 shows the impedance plots for $Ti_{1-x}Al_xN$ coated samples with 1 hr exposure time. Table 3 shows the results for other exposure times as R_p polarization resistance values which correspond to the low-frequency impedance limit adjusted for solution resistance. The electrode with $Ti_{1-x}Al_xN$ coating 6 showed some oscillations in corrosion potential; impedance variations for that type of coating were conducted at a higher amplitude of the alternating current signal and within a narrower frequency band.

Table 3: Polarized resistance of $Ti_{1-x}Al_xN$-coated samples after testing with various exposure times in 0.3% NaCl solution

Coating No.	R_p, kΩcm^2 with 0.3% NaCl exposure time, hr		
	1	2	3
1	150	98.5	-
2	59.0	-	-
3	115	56.0	-
4	39.5	16.6	10.9
5	110	73.0	57.5
6	34.8	38.6	17.4
TiN	62.2	33.0	23.7
X12M steel	2.5	1.9	-

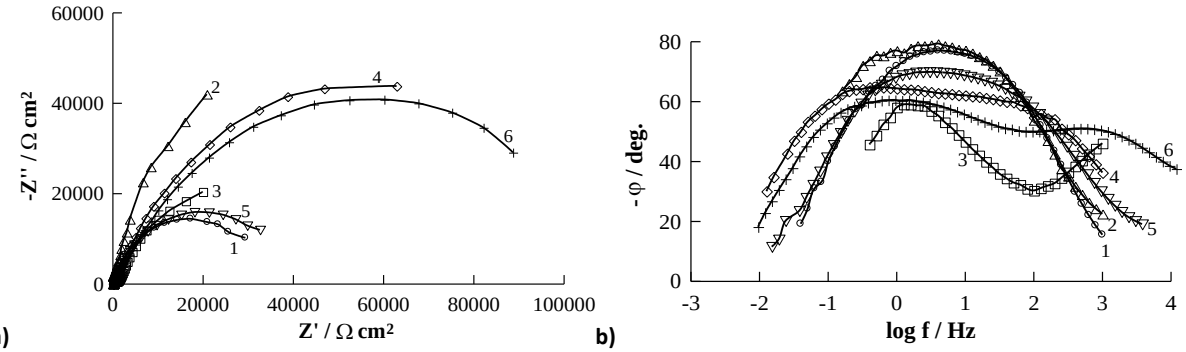

Figure 3: Nyquist plots (a) and Bode plots (b) for X12M steel with $Ti_{1-x}Al_xN$ coating in 0.3% NaCl solution under corrosion potential with 1 hr electrode exposure time. Curve numbers correspond to coating numbers in Tables 1 and 2

The shape of Nyquist plots for $Ti_{1-x}Al_xN$ coated samples is also close to the semicircle (Fig. 3a), however the Bode plots have quite a diverse appearance (Fig.3b), i.e. some details of impedance spectra within the high frequency band cannot be seen on the Nyquist plots but can be noticed on the Bode plots. The

ISSN: 0975-8585

Bode plots for $Ti_{1-x}Al_xN$ coated electrodes can be divided into two groups: 1) nearly symmetrical bell-shaped curves and 2) curves that have two overlapping peaks (coatings 2, 3 and 5).

The impedance of all $Ti_{1-x}Al_xN$ coatings in 0.3% NaCl solution declines in time (Tab.3), however the R_p rate of decline depends on the process conditions of coating deposition. Coating 1 has high values of polarization resistance which decline in time relatively slowly. Coating 3 also shows high initial R_p values, however, during the 2-hour exposure period, the polarized resistance for that type of coating drops to approximately 1/3 of its original value. The polarized resistance of all $Ti_{1-x}Al_xN$ coatings is higher than that of the substrate material (Tab.3), i.e. all the $Ti_{1-x}Al_xN$ coatings have a higher corrosion resistance compared to X12M steel. Coatings 1, 3 and 5 have the highest $R_p/R_{p,s}$ values, where $R_{p,s}$ is polarized resistance of the substrate.

The impedance of TiN-coated electrode in 0.3% NaCl solution was measured for comparison. The Nyquist plot for the TiN coating is close in shape to a semicircle with the centre below the X axis, while the Bode plot does not have a symmetric shape (Fig. 4).

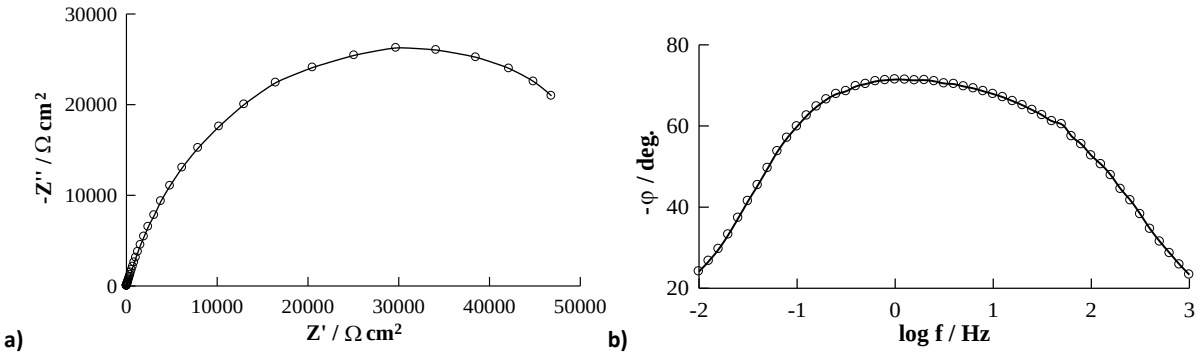

Figure 4: Nyquist plots (a) and Bode plots (b) for TiN coatings in 0.3% NaCl solution with 1 hr exposure time

To interpret the impedance of steel substrates with TiN or $Ti_{1-x}Al_xN$ coatings under corrosion potential, an equivalent circuit is normally used, as shown in Figure 5 [1, 2, 5 and 6]. Here R_s is solution resistance, R_{pore} is solution resistance in coating pores, R_p and C_d are polarized resistance and capacity of the double layer on substrate in coating pores and C_c is coating capacity. This model assumes that the electrode processes are completely concentrated in pores (on the pore bottom) and that the coating yields a purely capacitive response (like insulator film).

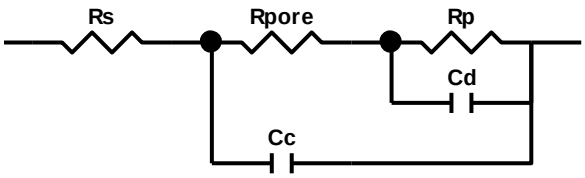

Figure 5: Equivalent electric circuit of a porous-coated electrode

Technically, this circuit (with elements of the CPE stationary phase instead of the C_d and C_c capacities) provides a satisfactory description of the experimental impedance spectra ($\chi^2 \leq 5\ 10^{-4}$), both when the Bode plot has two overlapping peaks and when it has only one maximum. Table 4 lists the values of the equivalent circuit (Fig.5) for a single value of electrode exposure time.

$$Y_{CPE} = Q(j\omega)^p ,$$

where Q and p are parameters in the CPE impedance expression.

ISSN: 0975-8585

Table 4: Equivalent circuit parameter values for 1 hr electrode exposure time in saline and calculated *P* values for coatings

Coating no	R_{pore}, Ω·cm^2	R_p, kΩ·cm^2	Q_d, μF cm^{-2}c^{p-1}	p_d	Q_c, μF cm^{-2}c^{p-1}	p_c	*P* from (1)	*P* from (2)
1	150	137.0	17.0	0.864	6.8	0.980	$3.6\cdot10^{-3}$	$1.3\cdot10^{-4}$
2	1690	64.3	12.5	0.834	3.6	0.705	-	$2.6\cdot10^{-5}$
3	5020	143.2	8.2	0.842	41.2	0.752	$1.0\cdot10^{-2}$	$9.5\cdot10^{-6}$
4	1080	40.2	10.4	0.817	34.6	0.841	$6.2\cdot10^{-2}$	$1.8\cdot10^{-5}$
5	1160	128.6	15.1	0.769	21.0	0.697	$3.4\cdot10^{-2}$	$2.3\cdot10^{-5}$
TiN	560	68.8	18.3	0.801	47.3	0.841	$9.4\cdot10^{-3}$	-

However, the following can be pointed out. The porosity of *P* coatings calculated from R_p values based on ratio (1) [4, 6] proves to be significant (Tab.4), which does not agree with the observed coating structure (Tab.2).

$$P = \left(\frac{R_{p,s}}{R_p} \right) \cdot 10^{-\Delta E_{corr} / b_a} , \qquad (1)$$

where $R_{p,s}$ and R_p are, respectively, polarized resistance of the substrate material and coated sample, ΔE_{cor} is corrosion potential difference between coated and uncoated substrates, and b_a is anodic Tafel slope for steel substrate.

On the other hand, the *P* value can be derived from expression (2) which follows from expression (3) for solution resistance in pores [6].

$$P = \frac{\rho\delta}{R_{pore}} , \qquad (2)$$

$$R_{pore} = \frac{\rho\delta}{P} , \qquad (3)$$

where ρ is resistivity of electrolyte solution and δ is coating thickness.

If we use ρ = 190 Ω cm for 0.3% NaCl solution at working temperature, the calculated values of $P \leq 0.01\%$ (Tab.4) will be by 2 or 3 orders of magnitude higher than the *P* values derived from ratio (1). Moreover, the highest *P* values from ratio (2) have been obtained for $Ti_{1-x}Al_xN$ coating 1 with the least defective structure (Tab.2), which looks improbable.

The Q_d values on the surface area occupied by pores are quite high (Tab.4). Consequently, the Q_d/P values are significantly higher than those for the double-layer capacity (Q_d parameter) of uncoated steel substrate.

The C_c coating capacity is determined by expression [6]:

$$C_c = \varepsilon_0\varepsilon(1-P)/\delta , \qquad (4)$$

where ε is coating permittivity.

Thus, to calculate the C_c value, we use the formula for a plate capacitor with an insulating layer between its coatings. The conductivity of $Ti_{1-x}Al_xN$ coating is visibly lower than that of TiN coating (according to [7], the resistivity of $Ti_{1-x}Al_xN$ coating is 225 to 317 Ω/sq (depending on the conditions of coating application) against 1 Ω/sq for TiN-coating), however it is sufficiently high and $Ti_{1-x}Al_xN$ coating is not an insulator.

Therefore, using the porous coating model (Fig.5) in the above physical sense of equivalent circuit parameters does not produce any consistent results.

ISSN: 0975-8585

If the experimental data agree with the equivalent circuit in Figure 5, they must also be described by the equivalent circuit in Figure 6 which is identical with the circuit in Figure 5 in the impedance frequency characteristics [8]. However, the equivalent circuit in Figure 6 has a different physical sense. This equivalent circuit can correspond to an electrode with conductive poreless coating where partial anodic and cathodic reactions on the coating/solution border proceed with activation control, while the adsorbed intermediate substance is involved in one of the reactions (e.g. the anodic one). In this case, the R_a and C_a elements are engaged in the anodic reaction, while both reactions contribute to the R_p resistance.

If an equivalent circuit is used as shown in Figure 6, the differences in polarized resistance and corrosion rate can be linked to the differences in chemical composition of the $Ti_{1-x}Al_xN$ coatings. This agrees with the existence of correlation between R_p and Al content in the coating (see Tab. 2 and 3). Previously in papers [9-12], the impedance of TiN, ZrN, and $Ti_xZr_{1-x}N$ coatings in alkaline conditions at E_{cor} and under anodic potentials was also explained by electrochemical processes on the coating/solution border without assuming any significant influence of pores on the electrochemical behaviour of the electrode.

The anode polarization curves for some coatings are shown in Figure 7. One can see that if E = const, the anode currents on coated samples are much higher than those on the substrate. Table 5 shows the i_{cor} corrosion currents derived by extrapolation from anode polarization of curves in E – lg$i$ coordinates up to the corrosion potential. The i_{cor} abatement correlates with the variation of polarization resistance measured under corrosion potential. For example, $Ti_{1-x}Al_xN$ coating 1 reduces i_{cor} by 43 times and increases R_p by 51 times.

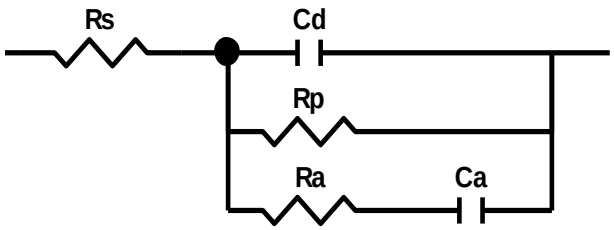

Figure 6: Equivalent circuit for the electrode with poreless conductive coating under corrosion potential

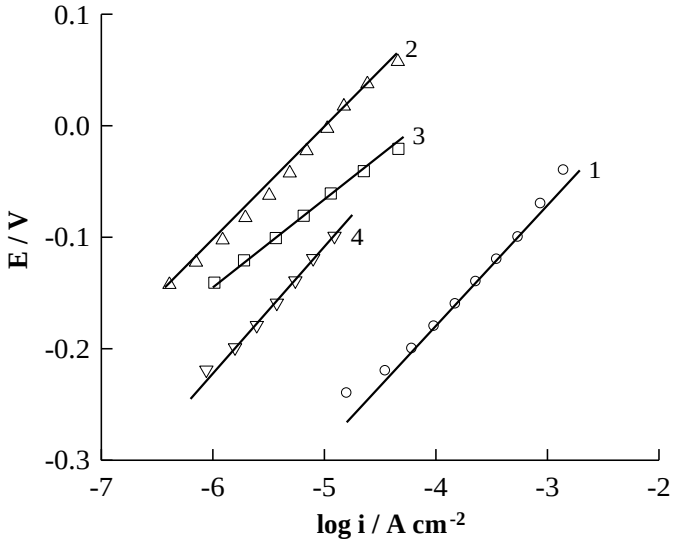

Figure 7: Anode polarization curves in 0.3% NaCl solution

Curve 1 – X12M; Curve 2 – $Ti_{1-x}Al_xN$ coating 1; Curve 3 – $Ti_{1-x}Al_xN$ coating 3; Curve 4 – $Ti_{1-x}Al_xN$ coating 5

ISSN: 0975-8585

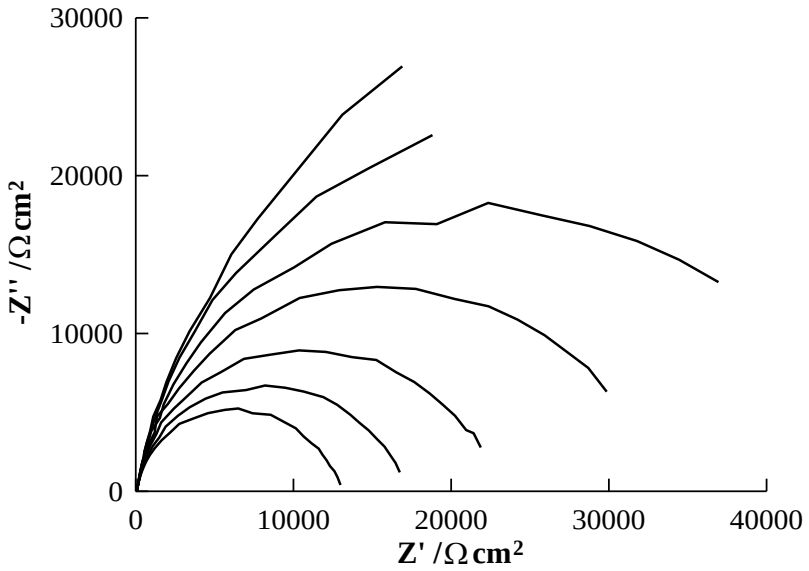

Figure 8: Nyquist plots for $Ti_{1-x}Al_xN$ coating 1 in 0.3% NaCl solution

The top curves correspond to electrode potentials from -0.14 to -0.02 B with 0.02 V interval

Table 5: Corrosion current density in 0.3% NaCl solution derived from polarization curves

Sample	i_{cor}, μA/cm^2
X12M	16.0
coating 1	0.37
coating 3	0.39
coating 5	0.63

The impedance spectra of anode-polarized samples made of coated X12M steel (рис.8) are close to semicircles with the centre below the X axis. The shape of impedance spectra does not change with the electrode potential (within the studied *E* interval). Therefore, we can say that the mechanism of anode process on the studied samples does not vary within the explored range of potentials and that the kinetics of anode process is determined by the stage of charge transfer.

The defectiveness of $Ti_{1-x}Al_xN$ coatings applied by PMS on X12M steel is reduced, while the Al content in coatings grows with the increase in MSS power and in nitrogen content in the N_2 + Ar gas mixture (from 7% N_2 to 12% N_2). Polarization resistance of $Ti_{1-x}Al_xN$-coated electrodes in 0.3% NaCl solution under corrosion potential correlates with the content of aluminum and $Ti_3Al_2N_2$ phase in coatings. $Ti_{1-x}Al_xN$ coating 1 with a dense ordered columnar defect-free structure and 20–50 nm crystallite diameter, maximum volume fraction of $Ti_3Al_2N_2$ phase (86 %) and Al concentration ($Ti_{0,62}Al_{0,38}N$) shows the highest corrosion resistance. For this type of coating, polarization resistance has high values and slowly declines in time. Coatings 3 and 5 with a dense orderly columnar structure but lower Al content are characterised by slightly smaller R_p values, compared to coating 1. The existence of isolated surface defects (coating 5) contributes to the decrease in R_p. $Ti_{1-x}Al_xN$ coatings 2, 4 and 6 with a cell structure, surface defects and lower Al concentration are characterised by lower R_p values. $Ti_{1-x}Al_xN$ coatings 1, 3 and 5 with a high content of $Ti_3Al_2N_2$ phase are superior to TiN coatings in corrosion resistance in 0.3% NaCl solution.

ACKNOWLEDGEMENTS

Work is performed in Perm National Research Polytechnic University with support of the Russian Ministry of Education and Science (contract № 02.G25.31.0068 from 23.05.2013 as part of measures to implement the decisions of the Russian Government № 218).

ISSN: 0975-8585

REFERENCES

[1] RM Souto, H Alanyali. Corr Sci 2000;42:2201.
[2] VKW Grips, HC Barshilia, VE Selvi, Kalavati KS Rajam. Thin Solid Films 2006;514:204.
[3] XZ Ding, ALK Tan, XT Zeng, C Wang, T Yue, CQ Sun. Thin Solid Films 2008;516:5716.
[4] V Chawla. J Mater Sci Eng A 2013;3(1):22-30.
[5] C Liu, Q Bi, A Leyland and A.Matthews. Corr Sci 2003;45:1243.
[6] C Liu, Q Bi, A Leyland and A Matthews. Corr Sci 2003;45:1257.
[7] M-H Park, S-H Kim. Trans Nonferrous Met Soc China 2013;23:433.
[8] IM Novoselskii, NN Gudina, YI Fetisov. Electrochem 1972;8:565.
[9] II Zamaletdinov, VI Kichigin, AL Kameneva, AA Onyanov, AY Klochkov. Corr Mater Prot 2010;7:34.
[10] II Zamaletdinov, VI Kichigin, AL Kameneva, AY Klochkov. Corr Mater Prot 2011;6:32.
[11] Kichigin VI, AL Kamenev, AA Onânov, Zamaletdinov II, Klochkov AY. Corr Mater Prot 2011;10:35.
[12] AL Kameneva, II Zamaletdinov, VI Kichigin. Corr Mater Prot 2013;1:29.